The Miniaturization of an Optical Absorption Spectrometer for Smart Sensing of Natural Gas

Ayerden, N. Pelin; Wolffenbuttel, Reinoud F.

DOI
10.1109/TIE.2017.2719600

Publication date
2017

Document Version
Final published version

Published in
IEEE Transactions on Industrial Electronics

The Miniaturization of an Optical Absorption Spectrometer for Smart Sensing of Natural Gas

N. Pelin Ayerden, *Member, IEEE*, and Reinoud F. Wolffenbuttel, *Senior Member, IEEE*

***Abstract*—Natural gas is the primary energy resource in both households and industry. Due to the molecular similarity of the main constituents, i.e., hydrocarbons, composition analysis of natural gas requires a highly selective and sensitive measurement technique. Smart sensing of natural gas in a large energy grid favors the use of methods that provide low unit cost in high-volume production, such as on-chip devices that can be micromachined at the wafer level, while maintaining the performance of complex benchtop instruments. Optical absorption spectroscopy with wide-band optical filters offers a comparable performance in a smaller footprint. However, the gas cell, where the absorption takes place, challenges the miniaturization of the spectrometer. This paper presents two approaches with analysis and experimental validation to integrate the gas cell and the linear variable optical filter (LVOF) at the wafer level. The first approach uses 45° inclined mirrors to steer the light beam through the sample gas, while the second approach, the gas-filled LVOF, functionally integrates the gas cell into the resonator cavity of the filter. Both devices are self-referenced and compatible with fabrication in a CMOS process, and therefore highly suitable for smart gas sensing.**

***Index Terms*—Gas sensor, microspectrometer, mid-infrared (IR), natural gas, optical absorption spectroscopy.**

I. Introduction

THE increasing international gas trade leads to natural gas mixtures of variable composition. Moreover, the trend toward the use of sustainable resources encourages the addition of biogas in the gas grid. All these changes necessitate composition measurements at industrial facilities, gas distribution points and households for safe and clean combustion, thereby, implying a high-volume application [1]. This requires small, autonomous, low-cost, and smart gas sensors that can analyze the measurement data on-site and communicate with the user. Silicon sensor fabrication can be tailored to be compatible with the CMOS technology, allowing the on-chip integration of the sensing element and the electronics, while the simultaneous processing of a batch of wafers brings high-volume production at low unit cost [2]. However, miniaturizing the sensors to the wafer level and maintaining the performance of their benchtop counterparts concurrently is challenging, especially when the sensitivity to the sample is related to the dimensions of the sensor.

In gas sensing, the composition of a sample mixture is measured by monitoring the change in either the chemical composition or a specific physical property of the sensing element in response to an interaction with the sample [3]. Metal-oxide gas sensors measure the change in electrical conductivity of semiconductors during the adsorption and desorption of gases [4]. Despite their high sensitivity and low cost, the dependency of the optimum operation temperature of the sensor on the sample is a limiting factor [5]. Moreover, these sensors suffer from long recovery periods, which makes them undesirable for applications where fast detection is required. In mass sensors, the sample binds with a chemically selective layer on an oscillator and the change of mass is monitored by measuring the changes in the oscillating behavior of, for instance, a cantilever [6]–[8]. Coating the oscillators with chemically active layers improves the sensor selectivity; however, it also increases the complexity of device fabrication. Since the operation of the sensor is based on binding the gas molecules to be measured, usually to the cantilever surface, the slow adsorption and desorption of the sample degrades the performance of especially the polymer-based devices [9].

Thermal gas sensors measure either the gas-specific thermal conductivity, using the thermal conductivity detector (TCD), or the gas-specific energy, using the calorimetric sensor [10]. In the TCD, an electric current is fed through a resistor and the injected heat results in a localized temperature increase that is measured using the same resistor or a thermocouple between the heater and a cooling rim [11], [12]. The temperature difference, at a given amount of heat introduced in the system, decreases with increasing thermal conductivity of the surrounding gas, because of a relatively high heat loss. For proper operation, the thermal conductivity of the substrate should be lower than that of the gas. In the calorimetric sensor, the local temperature increase due to heat generation by the combustion of the gas at the surface of a temperature sensor is measured [13]–[15]. A resistor or a membrane with an integrated resistor that is coated with a layer of a catalytic material to enable combustion of the gas at a certain elevated temperature, is generally used. The device is also referred to as a "(catalytic) pellistor" (note that, confusingly, the TCD is sometimes referred to as a "thermal conductivity pellistor"). The resistor is used as a heater to initiate the combustion at the well-defined elevated temperature and the increase of membrane temperature beyond that operating temperature is measured,

Manuscript received November 27, 2016; revised March 13, 2017; accepted June 8, 2017. Date of publication June 23, 2017; date of current version October 24, 2017. This work was supported by the Dutch technology foundation STW under Grant DEL.11476. *(Corresponding author: N. Pelin Ayerden.)*

The authors are with the Microelectronics Department, Delft University of Technology, 2628 CD Delft, The Netherlands (e-mail: n.p.ayerden@tudelft.nl; r.f.wolffenbuttel@tudelft.nl).

Color versions of one or more of the figures in this paper are available online at http://ieeexplore.ieee.org.

Digital Object Identifier 10.1109/TIE.2017.2719600

using either the same heater resistor or a thermopile between the membrane and the outer cooling rim [16]. However, catalytic sensors suffer from poisoning from certain types of compounds such as sulfur (H_2S), which inhibits the response of the sensor to combustible gases [17]. Therefore, despite their simple operating principle and low cost, catalytic pellistors put a prior condition on the sample set and are not capable of distinguishing between highly similar molecules such as hydrocarbons. Thermal conductivity-based devices can measure only binary mixtures, where the sample is composed of merely two gases [18]. Hence, in spite of its simplicity, reliability, and low cost, TCDs are not suitable for distinguishing constituents of a sample with complex composition due to the limited selectivity of the method. However, the sensitivity of a TCD makes it highly suitable as the end detector in a gas chromatograph, in which the column is used to separate the components to provide selectivity [19].

Optical absorption spectroscopy is a widely used quantitative analysis method for the identification of fluids [20], [21]. In this technique, the light is passed through a sample and the spectral distribution of the intensity of the transmitted light is measured with respect to the spectrum of the light source. Since the spectral distribution of absorption is unique to each molecule, the composition of the sample can be quantitatively identified by comparing the change in intensity through absorption to a spectral database using multivariate analysis techniques [22]. Its nondestructive and self-referencing properties, in addition to high selectivity and sensitivity, render optical absorption spectroscopy a highly suitable method for smart gas sensing [23].

An absorption spectrometer for gas analysis is essentially composed of a light source, a wavelength-selective element, a gas cell, and a detector. A wideband optical filter as a wavelength-selective element is highly suitable for miniaturization at the wafer level. However, the dimensions of the gas cell, where the sample to be measured is stored, limit the miniaturization due to the minimum path length requirement for a detectable absorption. In this paper, two different approaches for the composition measurement of natural gas in the mid-infrared (mid-IR) using on-chip optical absorption spectroscopy based on a wideband filter and a wafer-scale gas cell are introduced.

II. Optical Absorption Spectroscopy at the Wafer Level

Selectivity and sensitivity are the most important parameters in spectroscopy that define how well the components in a sample are distinguished and what the minimum detectable concentration is. A spectrometer that operates in a wide wavelength range allows for distinguishing materials with distinct spectral features, while a spectrometer with high resolving power enables differentiating samples with highly similar spectral response. Therefore, selectivity toward a wide range of samples requires a spectrometer with both high resolving power and a wide wavelength range.

The concentration sensitivity depends not only on how sensitive the detecting element is, but also on how sharp the spectral features of the sample are resolved and how efficient the interaction between the light and the sample is. The latter two are described by the Beer–Lambert law, where the absorbance of light that propagates through a sample is a linear function of the concentration, the absorption coefficient of the sample, and the length of the optical absorption path [24]. Hence, for a given detector sensitivity, the sensitivity to sample concentration can be improved by enhancing the resolution of the spectrometer to resolve higher values of the absorption coefficient and by elongating the optical absorption path.

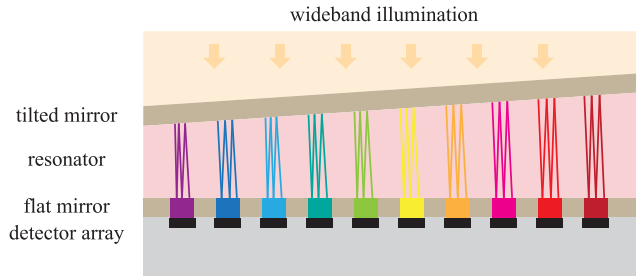

Fig. 1. Operation principle of LVOF. The wideband illumination is separated into different wavelengths along the length of the filter and the transmitted intensity is measured by the detector array underneath.

The linear variable optical filter (LVOF) is a wideband wavelength-selective element that can separate the incident light into different wavelengths spatially [25]. It is an interference filter that is composed of a tapered resonator layer sandwiched between a flat and a tilted mirror as shown in Fig. 1. The thickness of the resonator layer determines the wavelength to be transmitted through the device; hence, when the filter is combined with a detector array, a wideband spectral response can be measured along the length of the filter.

The LVOF can be designed to have a high resolving power to improve the selectivity and the sensitivity of a spectrometer. The elongation of the absorption path at wafer scale is achieved by either steering the light along the surface of the wafer using 45° inclined mirrors, or by using the resonator cavity of the LVOF as a gas cell and exploiting multiple reflections between highly reflective mirrors. The following sections describe both approaches with experimental results.

III. On-Chip Optical Absorption Path Using Planar Mirrors

The first approach toward building an on-chip microspectrometer is directed to the integration of different functional components on two separate wafers as shown in Fig. 2. One of the wafers hosts the light source as well as the combination of the LVOF and the detector array. The other wafer is composed of two 45° inclined mirrors facing each other, while the space in-between is used as the gas cell.

A. Fabrication and Optical Efficiency Analysis of 45° Inclined Mirrors

Fabrication of trenches in an Si wafer with 45° tapered sidewalls using wet etching methods for efficient fiber coupling has been previously reported [26]. By aligning the etch mask in the <100> direction in a (100) Si wafer, 45° inclined mirrors can

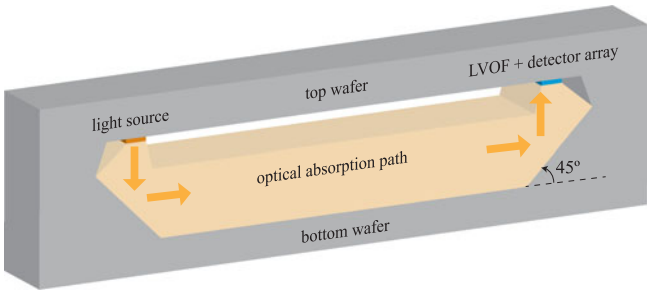

Fig. 2. Schematic illustration of a wafer-scale microspectrometer using an on-chip gas cell with 45° inclined mirrors.

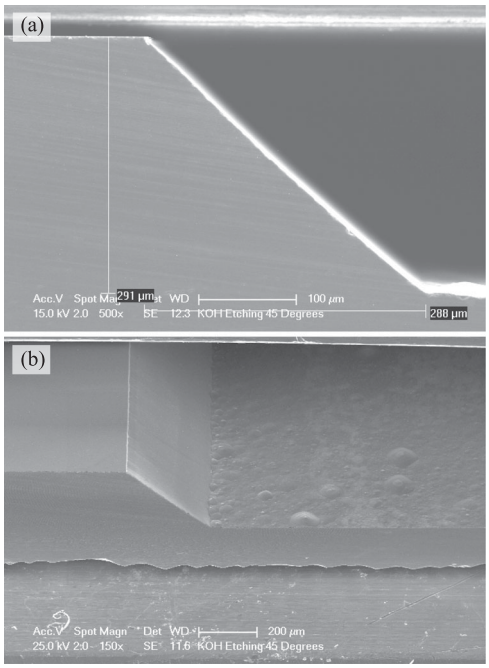

Fig. 3. (a) Side and (b) oblique view of the SEM images of 45° inclined mirrors etched 290 μm deep using 2 M KOH + 60 ppm Triton X-100 at 90 °C.

be fabricated on the {110} planes by wet etching [27]. Moreover, by adding a surfactant such as Triton X-100 to the etching solution, the surface quality of the mirror can be improved considerably [28]. The SEM images of a 45° inclined mirror that is etched 290 μm deep using 2 M KOH + 60 ppm Triton X-100 at 90 °C are shown in Fig. 3. When coated with a reflective layer in the mid-IR, such as gold or aluminum, these mirrors would be able to steer the IR light beam along the surface of a wafer [29].

The surface roughness of a 45° inclined mirror fabricated by through-wafer etching is measured using atomic-force microscopy. The mirror is diced along its upper edge and placed on a 45° inclined wedge to achieve a horizontal surface for roughness analysis. Measurements at different areas on the surface of the mirror revealed a root-mean-square roughness below 15 nm. Considering the optical flatness limit of $\lambda/10$, where λ represents the wavelength, and the mid-IR wavelength range required for the application, the surface quality of the mirrors is safely within the limits.

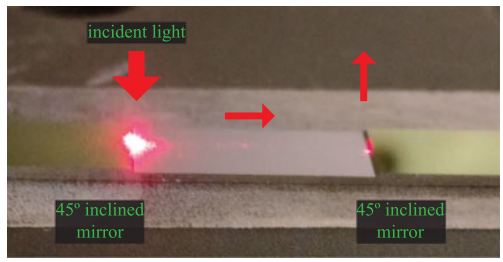

Fig. 4. Collimated red HeNe laser beam at 632 nm wavelength propagating along the fabricated gas cell.

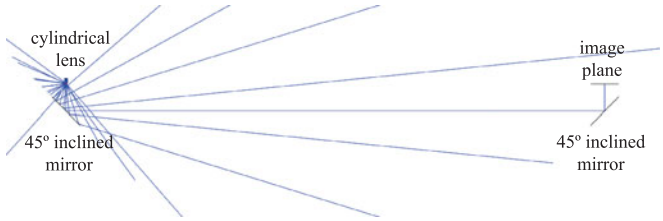

Fig. 5. Zemax layout of the on-chip optical absorption path with 45° inclined mirrors.

The fabricated on-chip gas cell is investigated using a red HeNe laser at 632 nm wavelength as shown in Fig. 4. The normally incident collimated light beam is reflected off the first 45° inclined mirror toward the optical absorption path. After propagating along the 10 mm long path, the light beam is reflected back by the second 45° inclined mirror. The size difference between the mirror and the incident spot in addition to the limited reflectivity of Si in the visible range result in a reflected light beam with low intensity. However, this qualitative measurement demonstrates that the on-chip gas cell is suitable for steering the light beam along a predefined path as required in this application.

The power efficiency of the microspectrometer with 45° inclined mirrors is analyzed using the ray tracing software, Zemax (Zemax, LLC, USA). The wavelength distribution is neglected and the power impinging on the filter is taken into consideration for analysis. The simplified system consists of a light source, two 45° inclined mirrors with a 10 mm long optical absorption path in-between, and an image plane as shown in Fig. 5. The image plane represents the combination of the LVOF and the detector array. The light source is implemented as a cylindrical lens to replicate a filament-like blackbody emitter. The 3 mm long cylindrical lens has a diameter of 0.06 mm. The size of the 45° inclined mirrors is maximized to demonstrate the best-case efficiency. The largest mirror can be achieved by through-wafer etching, therefore the width of the mirror is selected as 0.74 mm, assuming a standard 4-in wafer thickness of 524 μm. The cylindrical lens and the image plane are placed 0.5 mm away from the 45° inclined mirrors.

The efficiency simulations are performed using the geometric image analysis based entirely on geometrical optics in the sequential mode of Zemax. Since the cylindrical lens represents the light source, the power observed at the remaining components is normalized to the power at the cylindrical lens. The power efficiency analysis results are given in Table I for

TABLE I
POWER EFFICIENCY ANALYSIS RESULTS

Optical component	Power efficiency (%)
Cylindrical lens	100
First mirror	33.29
Second mirror	1.24
Image plane	1.18

each surface. Only one-third of the emitted light reaches the first mirror and more than 95% of the light that is reflected off the first mirror diverges from the intended optical path. Finally, only 1.18% of the overall power ends up at the image plane in the best-case scenario. Although the power efficiency is maximized by increasing the size of the mirror via through-wafer etching, the robustness of the entire optical system deteriorates. In addition, the stray light that stems from the divergence of the beam renders the quantitative sample analysis, which is directly correlated to the absorption path length, inaccurate. With the limitations imposed by the fabrication tolerances, the efficiency of an on-chip microspectrometer system with 45° inclined mirrors decreases sharply when combined with a wideband emitter without any collimating optics.

The efficiency could be highly improved by collimating the light beam emitted from the source. This can be achieved either by replacing the 45° inclined mirrors with micromachined parabolic mirrors [30], or by combining the IR emitter with a collimating microlens array [31]. The solution with parabolic mirrors allows the fabrication complexity to be evenly distributed between the top and the bottom wafers, while the imperfections in the mirror profile could degrade the efficiency strongly. Microlens array fabrication is a well-established area, therefore these structures are less vulnerable to manufacturing tolerances. However, fabricating the microlens array directly on top of the IR emitter introduces additional complexity on the top wafer. Both approaches offer a compact optical absorption spectrometer, where an on-chip gas cell is formed effectively by steering the light beam along the surface of a wafer. The system can be easily tailored for applications with different concentration detection requirements by tuning the distance between the mirrors.

B. Spectral Performance of Mid-IR LVOFs

The distinctive optical absorption features of natural gas requires wavelength selection in the mid-IR. A first-order LVOF with a tapered SiO_2 resonator layer is designed and fabricated [32]. The thickness of the resonator varies between 1027 and 1301 nm, corresponding to the 3–3.8 μm wavelength range. The spectral response is measured using a benchtop FTIR spectrometer (Vertex 70, Bruker Optics, Germany) at 4 cm^{-1} resolution as shown in Fig. 6. The LVOF is mounted on a manual translational stage and placed at the sample plane of the instrument. To measure the spatial distribution of the spectral response, the smallest possible beam is directed at the LVOF and the filter is scanned along its length with 500 μm steps. At every measurement, 128 scans are averaged to improve the signal-to-noise ratio. Each transmission curve corresponds to a particular position along the length of the filter. A full width at half maximum (FWHM) resolution of approximately 80 nm is achieved.

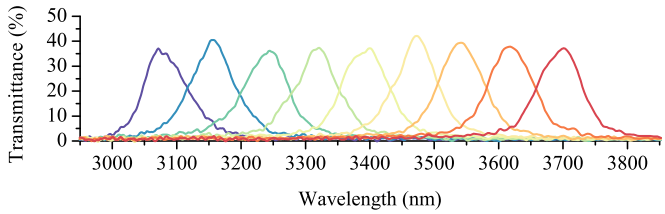

Fig. 6. Measured spectral response of a first-order mid-IR LVOF.

IV. GAS-FILLED LVOF

Miniaturization of an on-chip microspectrometer can be taken one step further by functionally integrating the LVOF and the gas cell, i.e., the gas-filled LVOF. The resonator layer of an LVOF, where wavelength selection occurs through the interference of light after multiple reflections between the mirrors, can be either a physical layer or a cavity. When the resonator cavity of an LVOF is used as a gas cell, multiple reflections serve not only to select the wavelength but also to enhance the interaction between light and the gas sample.

A. Optical Design

Cavity-enhanced methods exploit multiple reflections in high-finesse optical cavities that require the use of almost ideal reflectors ($R \approx 99.9\%$) [33]. This results in meters of effective optical absorption path and makes cavity-enhanced absorption spectroscopy (CEAS) a commonly used method in trace gas sensing [34]. However, this method necessitates the use of high power lasers as a light source; thus, limiting the miniaturization. In the gas-filled LVOF, instead of almost ideal mirrors, highly reflective mirrors ($R \approx 98.5\%$) are employed so that the requirements on the light source are moderated. Therefore, a μm-level physical cavity of a miniaturized microspectrometer can be elongated into an effective optical absorption path at the mm-level.

The main components of natural gas are hydrocarbons. These molecules have distinctive spectral features in the 3.1–3.6 μm wavelength range as shown in Fig. 7. To enhance the effect of cavity length elongation on absorption, highly reflective mirrors must be accompanied by a long physical cavity. This forces the LVOF to operate at a higher order; thus, limits the operating wavelength range. Therefore, the spectral band from 3.2–3.4 μm is selected due to the strongly distinguishing absorption features between hydrocarbons.

The spectral response of the LVOF is conventionally simulated by approximating the effect of the tapered resonator to an array of fixed Fabry–Perot (FP) filters with parallel mirrors. Such an approximation is valid for moderate mirror reflectivity and operating order. However, high operating order and high mirror reflectivity, as required for the gas-filled LVOF application, necessitates taking the taper angle of the cavity into account [36]. In contrast to an FP interferometer, the angle of reflection changes at every interaction between the light and the tilted

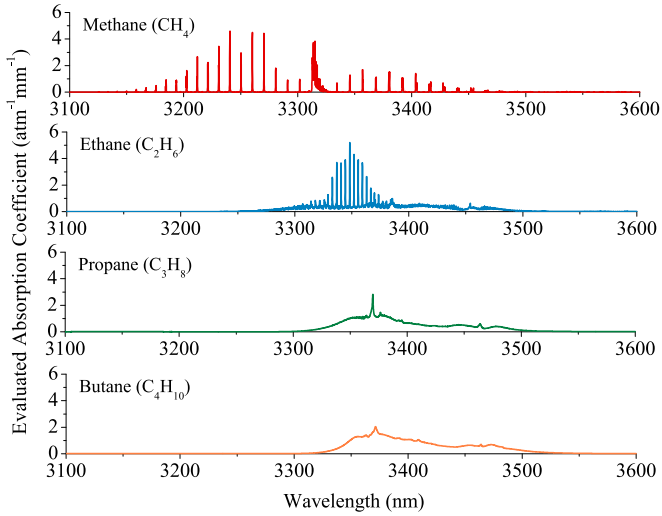

Fig. 7. Evaluated absorption coefficient spectra of methane, ethane, propane, and butane per unit pressure and optical absorption path extracted from PNNL database at 0.112 cm^{-1} resolution [35].

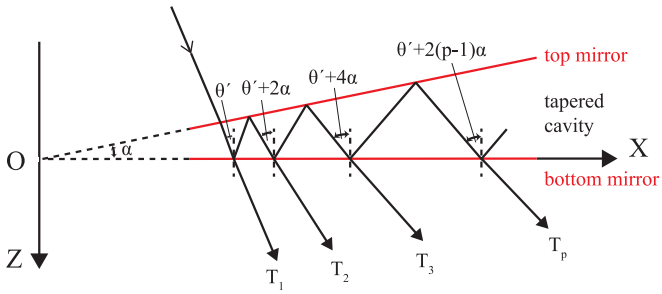

Fig. 8. Multiple reflections in Fizeau interferometer at a positive angle of incidence.

mirror in an LVOF. These multiple reflections cause the light beam to laterally shift and eventually walk off the tapered cavity. At demanding operating conditions, this walk off degrades the spectral performance of the filter in terms of both transmission and resolution. Therefore, an accurate assessment of the spectral behavior of the gas-filled LVOF requires the use of the Fizeau interferometer approach, where the taper in the cavity is taken into consideration.

Multiple reflections in a tapered cavity are shown in Fig. 8 for positive angle of incidence. For a taper angle of α and an incidence angle of θ', the angle of reflection within the cavity is defined as $\theta' \pm 2(p-1)\alpha$, where p represents the number of waves that are transmitted through the filter. The increase or the decrease, i.e., the selection of the $\pm$ sign depends on the direction of the incidence. A positive incidence away from the cavity apex (O) causes the angle of reflection to increase at every interaction, while a negative incidence toward the cavity apex results in a decreasing angle.

The phase difference between the pth and the directly transmitted waves can be calculated using (1) for both positive and negative incidence angles. The wavelength is represented by λ_0, while x indicates the position along the length of the filter and z is the distance between the filter and the point

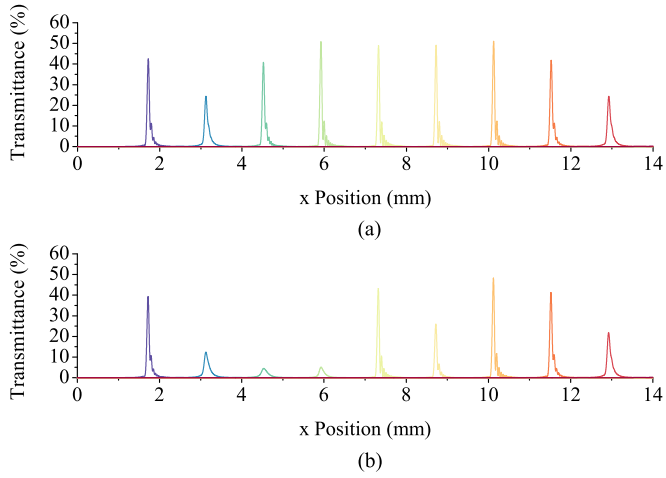

Fig. 9. Transmission response of the LVOF (a) without gas and (b) with methane in the cavity.

where the interference is observed. When the phase difference is combined with the reflectivity and transmissivity of the mirrors, the spectral response of the LVOF can be accurately estimated. To incorporate the effect of the optical absorption by the sample gas in the cavity, an exponential attenuation factor based on the absorption coefficient of the gas is introduced in the calculations for every reflection.

$$\delta_p = \frac{2\pi}{\lambda_0}\left(x\left[\sin\left(\theta' + 2(p-1)\alpha\right) - \sin\theta'\right] + z\left[\cos\left(\theta' + 2\left(p-1\right)\alpha\right) - \cos\theta'\right]\right) \quad (1)$$

A 14 mm long LVOF that operates at the 15th order in the 3.2–3.4 μm wavelength range is designed using the Fizeau interferometer approach. The highly reflective mirrors are implemented as Bragg reflectors, where alternating layers of IR-transparent thin-films with quarter-wavelength optical thickness are employed. Using three pairs of Si and SiO_2 thin-films, a mirror reflectivity varying from 98.5% to 99.5% is achieved. The fluctuations in the reflectivity originate from the fact that the tapered cavity is formed by combining a flat and a tapered mirror rather than integrating a flat and a tilted mirror. The tapered mirror is realized by tapering the first SiO_2 layer; hence, the change in the thin-film thickness results in a position-dependent reflectivity.

The nonparallelism of the mirrors turns the angle of incidence into an optimization parameter [37]. For a given z value, θ' can be selected to result in high transmittance and resolution. The position-dependent spectral response of the gas-filled LVOF is calculated for the 3.2–3.4 μm wavelength range using the Fizeau interferometer approach, as shown in Fig. 9. The position on the filter along the x-axis is scanned and the transmittance right after the filter is calculated for the incidence angle of -1.61°. The absorption coefficient of methane is extracted from the HITRAN database and evaluated with respect to the resolution of the device [38]. Based on the spectral distribution of the absorption coefficient of methane, the optical path length is elongated from the physical cavity length of 24–25.5 μm into the effective absorption path length that varies between 3.2 and 10.2 mm, theoretically.

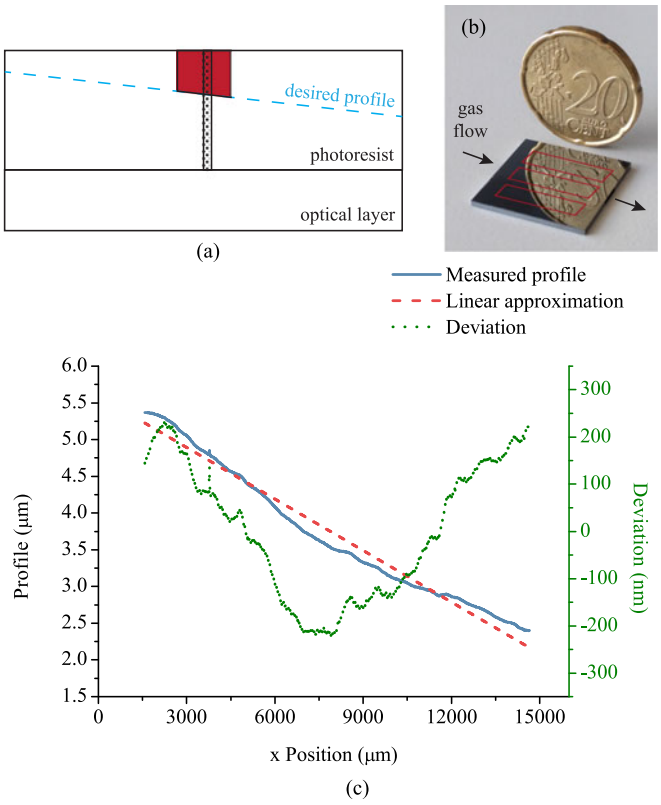

Fig. 10. (a) Schematic illustration of the principle used in the fabrication of a tapered optical layer. (b) Photograph of a die with three gas-filled LVOFs. (c) Measured profile of the tapered mirror compared with its linear approximation.

B. Device Fabrication

The fabrication of a gas-filled LVOF is based on manufacturing the flat and the tapered mirrors separately and subsequent wafer bonding [39]. The flat mirror is formed in a 30 μm deep KOH etched cavity. The depth of this wet-etched cavity defines the total thickness of the mirrors and the physical length of the resonator cavity. In a fixed FP filter, a slight change in these values due to fabrication tolerances would result in a wavelength shift in the spectral response and eventually degrade the performance of the sensor. The LVOF, on the other hand, is immune to such fabrication variations due to the linear taper of the resonator cavity. Therefore, if the fabrication tolerances would result in a different range of cavity length than specified, the entire expected spectral response would only shift along the length of the filter.

The flat mirror is fabricated by sputtering six alternate layers of Si and SiO_2. Later, 275 μm deep openings are etched on the frame around the mirror using deep reactive ion etching, for enabling gas inlet and outlet. Finally, the protective layers on the frame are removed and the wafer is prepared for bonding.

The tapered Bragg mirror is formed by tapering the first SiO_2 layer and then depositing the remaining thin-film layers on top. The height difference between the onset and the end of the tapered layer is defined by the variation in resonator length. Distinguishing hydrocarbons by their spectral signature in the 3.2–3.4 μm wavelength range requires a resonator length

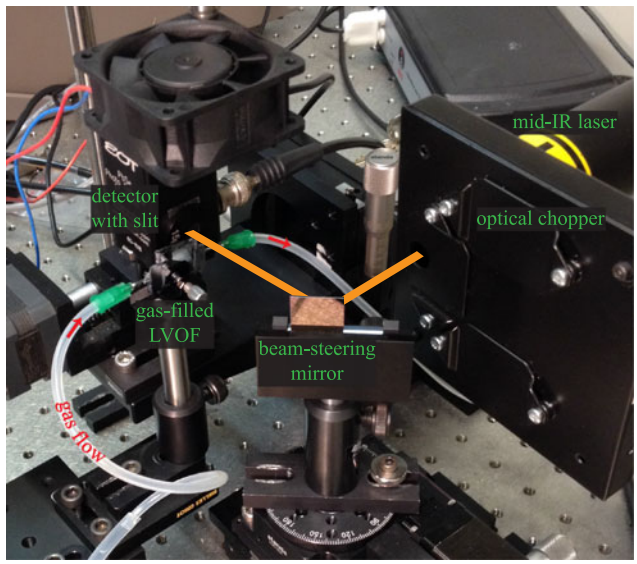

Fig. 11. Optical characterization setup.

changing from 24 to 25.5 μm, implying a level difference of at least 1.5 μm in the tapered mirror. This value is doubled to account for fabrication tolerances. As a result, a 14 mm long tapered SiO_2 layer with 3 μm level difference is fabricated.

The key step of this process is the fabrication of a tapered SiO_2 layer with a small taper angle and maintaining the same taper along the width of the layer to ensure sufficient light throughput. The fabrication of the tapered optical layer relies on the fabrication of a tapered photoresist followed by transfer etching [40]. The tapered resist profile is formed by low-cost methods using a conventional mask with linearly variable distanced trenches. The technique is based on the principle that the volume of a trench must be equal to the volume of the photoresist on both sides of the trench that must be removed to obtain the desired slope as shown in Fig. 10(a). After the photoresist is patterned, the wafer undergoes a thermal-chemical treatment to convert the photoresist layer with linearly variable distanced trenches to a smooth tapered structure. Then, this tapered resist layer is transferred to the underlying optical layer using one-to-one plasma etching. Finally, the openings for the gas flow are etched and wafers with flat and tapered mirrors are bonded. A die with three filters is shown in Fig. 10(b).

The performance of an LVOF with a resonator cavity is highly dependent on the profile of the mirrors. The deviation from the linear taper results in a nonuniform separation in the wavelength domain. Moreover, since interference occurs at different positions along the length of the filter, the localized deviation of the taper, i.e., surface deformation, has a significant effect on the quality of the interference. Therefore, the surface profile of the tapered Bragg mirror was measured using a stylus profiler prior to wafer bonding. A coarse pixel distribution in the detector array, such as 20 pixels over a length of 14 mm, results in a pixel size of 700 μm. As given in Fig. 10(c), the deviation from the ideal tapered profile at every 700 μm is within the limits of $\lambda/10$ surface deformation, given that the shortest wavelength in the system is 3200 nm. Also, the highly linear measured

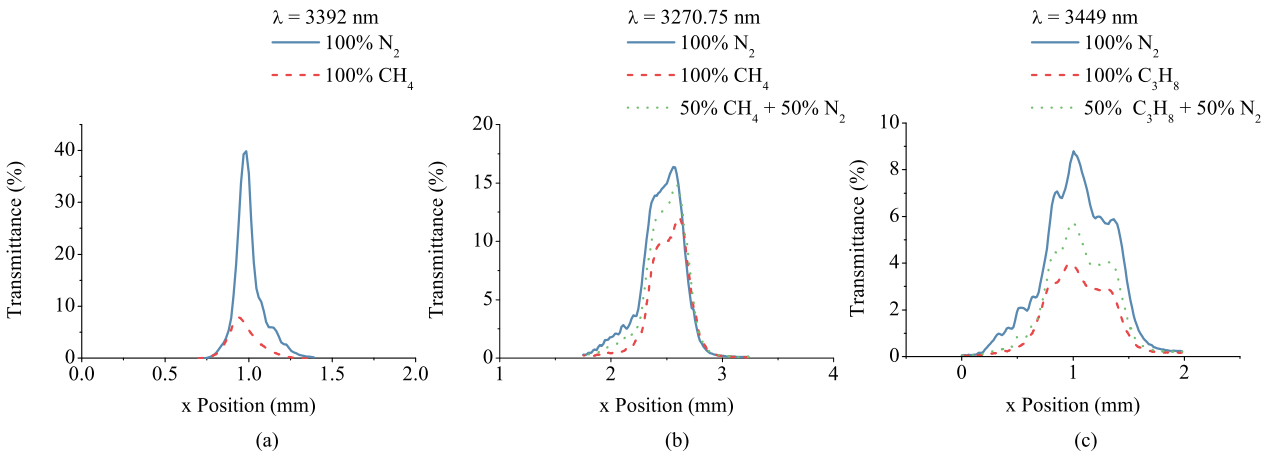

Fig. 12. Measured transmission response of the gas-filled LVOF (a) at 3392 nm wavelength with 100% methane and 100% nitrogen using a HeNe laser (b) at 3270.75 nm wavelength with 100% methane, 100% nitrogen as well as a mixture with 50% methane and 50% nitrogen using an experimental OPO laser and (c) at 3449 nm wavelength with 100% propane, 100% nitrogen as well as a mixture with 50% propane and 50% nitrogen using an experimental OPO laser. The actual x Position values at different measurements are not related.

profile of the tapered mirror allows for uniform separation of the wavelengths.

C. Characterization

The gas-filled LVOF is to be integrated with a wideband light source and a detector array in the final device. However, to investigate the spectral resolution limit, the device must be characterized using a light source with a spectral purity that is better than the resolution of the LVOF. Moreover, the spectral response of the device is susceptible to the cone angle of the light source [41]. Therefore, an optical setup with a high-resolution HeNe laser with collimated output at 3392 nm wavelength is built to measure the spectral response of the LVOF.

The benchtop optical characterization setup is shown in Fig. 11. The light beam emitted from the laser is chopped at 1 kHz to improve the signal-to-noise ratio at the detector. After the optical chopper, the incidence angle of the light beam that impinges on the gas-filled LVOF is selected using the beam-steering mirror. Later, the light transmitted through the LVOF is collected at the large-area detector, where a 15 μm wide slit is employed for spatial filtering to replicate the effect of a pixel in a detector array. The resonator cavity of the gas-filled LVOF is connected to the gas bottle via flexible tubes and dispensing tips. The gas flow is ensured by applying a slight pressure difference between the inlet and the outlet tubes.

The transmission behavior of the gas-filled LVOF is characterized by comparing the spectral distribution of the intensity with the sample gas to the reference measurement without the gas in the cavity. In a self-sustaining implementation, two identical gas-filled LVOFs must be employed, where a sealed filter with an empty cavity would serve as the reference and a filter with openings on the sides would measure the ambient gases. For the experimental validation on the other hand, the transmission through the same filter is first measured with the IR-inactive gas, nitrogen, as the reference and then the sample gas is flown through the cavity. The transmission curve is constructed by scanning the filter along its length at a step size of 15 μm.

The spectral response of the gas-filled LVOF at 3392 nm wavelength with methane and nitrogen is shown in Fig. 12(a). The interference is observed more than 6 mm away from the device at an optimum incidence angle of -8.8° and an FWHM resolution better than 5 nm is achieved. The 39.9% reference peak transmittance measured with nitrogen decreases down to 7.8% when methane is fed into the resonator cavity of the gas-filled LVOF. Considering the high absorption coefficient resolved by the laser, this translates into an effective optical absorption path of 1.58 mm.

The difference between the designed and measured effective absorption path length mainly stems from the operation principle of the CEAS method. In this technique, as the absorption of the sample becomes comparable to the cavity loss, the sensitivity improvement saturates [42]. In other words, the absorption of the sample begins to dominate the effective number of cavity passes. The absorption coefficient of methane that was resolved by the narrow-linewidth HeNe laser is higher than the value that would be achieved with the sole resolving power of the gas-filled LVOF. Therefore, the lower absorption coefficient gave rise to a higher number of reflections; hence, a longer effective optical absorption path in the simulations. Moreover, variations in the thickness of the Bragg mirror layers might cause a slight decrease in reflectivity; thus, a reduction in the effective absorption path length.

To investigate the wavelength selectivity of the gas-filled LVOF and its response to different hydrocarbons, measurements using an experimental optical parametric oscillator (OPO) laser in the mid-IR are performed [43]. The HeNe laser in the optical characterization setup is replaced with the OPO laser setup and collimating optics. The spectral response of the gas-filled LVOF with pure methane and nitrogen as well as their one-to-one dilution is measured at 3270.75 nm as shown in Fig. 12(b). Since the absorption coefficient of methane at this wavelength is lower compared to the value at 3392 nm, the absorption of methane is less significant. Despite that, the effect of both pure methane and the dilution was observed in the spectral response. Similarly, the spectral response of the gas-filled LVOF with

pure propane and nitrogen as well as their one-to-one dilution is measured at 3449 nm as shown in Fig. 12(c). Due to relatively high absorption coefficient of propane at this wavelength, pure sample gas in the cavity absorbs more than half of the incoming light. The transmission curve of the diluted gas is between the response of pure nitrogen and methane, as expected. These measurements with different hydrocarbons, including dilutions at various wavelengths, demonstrate the selectivity and the sensitivity of the gas-filled LVOF.

V. Conclusion

In this paper, two on-chip implementations of optical absorption spectroscopy for smart gas sensing were reported. In both implementations, the target is achieving the selectivity and sensitivity of sophisticated benchtop spectrometers at the wafer level using optical filters, while maintaining CMOS compatibility. Selectivity is acquired by the wide operating bandwidth and high resolution of the LVOF. To improve sensitivity on the other hand, the interaction between the light and the sample gas must be enhanced. The first on-chip microspectrometer uses 45° inclined mirrors to steer the light beam parallel to the wafer surface through the sample gas. By increasing the distance between the mirrors, the physical absorption length can be increased to improve the sensitivity of the spectrometer. In the gas-filled LVOF, the length of the microcavity is translated into an effective absorption path length at the mm-level through multiple reflections. Therefore, a sensitivity, which is beyond the value that is attainable given the dimensions of the device is obtained.

Both implementations impose strict limitations on the collimation of the light source. The microspectrometer with 45° inclined mirrors requires the light beam to be collimated to achieve a detectable intensity after propagating through the long absorption path, as well as to minimize the effect of stray light on spectral analysis. In a similar manner, the performance of the gas-filled LVOF is strongly affected by the divergence angle of the light source due to the high-order operation and the use of highly reflective mirrors. However, both systems offer high spectral performance when combined with a collimated light source.

The sensitivity of the on-chip microspectrometer with 45° inclined mirrors can be easily tailored for different applications, irrespective of the optical design of the LVOF, by changing the dimensions of the absorption path. The increased level of miniaturization in the gas-filled LVOF forces the absorption path length and the optical design of the LVOF to be interdependent. This necessitates an optimization of the tradeoff between selectivity and sensitivity. Therefore, the gas-filled LVOF offers the ultimate miniaturization at the expense of design simplicity, while the on-chip microspectrometer with 45° inclined mirrors allows for improving the sensitivity in exchange for increased device dimensions. Despite the minor differences, both devices revolutionize gas sensing in the mid-IR and bring cumbersome benchtop instruments to the wafer level. Thanks to the CMOS-compatible fabrication, these microspectrometers would be highly suitable for smart sensing of natural gas for both residential and industrial applications when combined with the electronic circuits.

References

[1] J. Leis and D. Buttsworth, "A temperature compensation technique for near-infrared methane gas threshold detection," *IEEE Trans. Ind. Electron.*, vol. 63, no. 3, pp. 1813–1821, Mar. 2016, doi:10.1109/TIE.2015.2495292.

[2] R. F. Wolffenbuttel, *Silicon Sensors and Circuits: On-chip Compatibility*. New York, NY, USA: Springer, 1996.

[3] F.-G. Banica, *Chemical Sensors and Biosensors: Fundamentals and Applications*. Hoboken, NJ, USA: Wiley, 2012.

[4] T. Seiyama, A. Kato, K. Fujiishi, and M. Nagatani, "A new detector for gaseous components using semiconductive thin films," *Anal. Chem.*, vol. 34, no. 11, pp. 1502–1503, Oct. 1962, doi:10.1021/ac60191a001.

[5] G. F. Fine, L. M. Cavanagh, A. Afonja, and R. Binions, "Metal oxide semi-conductor gas sensors in environmental monitoring," *Sensors*, vol. 10, no. 6, pp. 5469–5502, Jun. 2010, doi:10.3390/s100605469.

[6] J. Janata, *Principles of Chemical Sensors*. New York, NY, USA: Springer, 2010.

[7] H. J. Lee, K. K. Park, O. Oralkan, M. Kupnik, and B. T. Khuri-Yakub, "A multichannel oscillator for a resonant chemical sensor system," *IEEE Trans. Ind. Electron.*, vol. 61, no. 10, pp. 5632–5640, Jan. 2014, doi:10.1109/TIE.2014.2300031.

[8] H. Yu, P. Xu, X. Xia, D. W. Lee, and X. Li, "Micro-/nanocombined gas sensors with functionalized mesoporous thin film self-assembled in batches onto resonant cantilevers," *IEEE Trans. Ind. Electron.*, vol. 59, no. 12, pp. 4881–4887, Dec. 2012, doi:10.1109/TIE.2011.2173094.

[9] C. Yim *et al.*, "Adsorption and desorption characteristics of alcohol vapors on a nanoporous ZIF-8 film investigated using silicon microcantilevers," *Chem. Commun.*, vol. 51, no. 28, pp. 6168–6171, Mar. 2015, doi:10.1039/C5CC01315A.

[10] X. Liu, S. Cheng, H. Liu, S. Hu, D. Zhang, and H. Ning, "A survey on gas sensing technology," *Sensors*, vol. 12, no. 7, pp. 9635–9665, Jul. 2012, doi:10.3390/s120709635.

[11] P. Tardy, J.-R. Coulon, C. Lucat, and F. Menil, "Dynamic thermal conductivity sensor for gas detection," *Sens. Actuators B, Chem.*, vol. 98, no. 1, pp. 63–68, Mar. 2004, doi:10.1016/j.snb.2003.09.019.

[12] G. de Graaf, A. Abarca Prouza, M. Ghaderi, and R. F. Wolffenbuttel, "Micro thermal conductivity detector with flow compensation using a dual MEMS device," *Sens. Actuators A, Phys.*, vol. 249, pp. 186–198, Oct. 2016, doi:10.1016/j.sna.2016.08.019.

[13] J. G. Firth, A. Jones, and T. A. Jones, "The principles of the detection of flammable atmospheres by catalytic devices," *Combustion Flame*, vol. 20, no. 3, pp. 303–311, Jun. 1973, doi:10.1016/0010-2180(73)90021-7.

[14] P. N. Bartlett and S. Guerin, "A micromachined calorimetric gas sensor: an application of electrodeposited nanostructured palladium for the detection of combustible gases," *Anal. Chem.*, vol. 75, no. 1, pp. 126–132, Jan. 2003, doi:10.1021/ac026141w.

[15] C. Hagleitner, D. Lange, A. Hierlemann, O. Brand, and H. Baltes, "CMOS single-chip gas detection system comprising capacitive, calorimetric and mass-sensitive microsensors," *IEEE J. Solid-State Circuits*, vol. 37, no. 12, pp. 1867–1878, Dec. 2002, doi:10.1109/JSSC.2002.804359.

[16] A. W. van Herwaarden, P. M. Sarro, J. W. Gardner, and P. Bataillard, "Liquid and gas micro-calorimeters for (bio)chemical measurements," *Sens. Actuators A, Phys.*, vol. 43, no. 1, pp. 24–30, May 1994, doi:10.1016/0924-4247(93)00658-Q.

[17] Y. Deng, T. G. Nevell, R. J. Ewen, and C. L. Honeybourne, "Sulfur poisoning, recovery and related phenomena over supported palladium, rhodium and iridium catalysts for methane oxidation," *Appl. Catal. A, Gen.*, vol. 101, no. 1, pp. 51–62, Jul. 1993, doi:10.1016/0926-860X(93)80137-F.

[18] B. G. Liptak, *Analytical Instrumentation*. Boca Raton, FL, USA: CRC Press, 1994.

[19] K. Dettmer-Wilde and W. Engewald, *Practical Gas Chromatography: A Comprehensive Reference*. Berlin, Germany: Springer, 2014.

[20] N. V. Tkachenko, *Optical Spectroscopy: Methods and Instrumentations*. Amsterdam, The Netherlands: Elsevier, 2006.

[21] A. V. Fernandes, V. F. Cardoso, J. G. Rocha, J. Cabral, and G. Minas, "Smart-optical detector CMOS array for biochemical parameters analysis in physiological fluids," *IEEE Trans. Ind. Electron.*, vol. 55, no. 9, pp. 3192–3200, Sep. 2008, doi:10.1109/TIE.2008.927962.

[22] K. Varmuza and P. Filzmoser, *Introduction to Multivariate Statistical Analysis in Chemometrics*. Boca Raton, FL, USA: CRC Press, 2016.

[23] J. Hodgkinson and R. P. Tatam, "Optical gas sensing: a review," *Meas. Sci. Technol.*, vol. 24, no. 1, Jan. 2013, Art. no. 012004, doi:10.1088/0957-0233/24/1/012004
[24] D. F. Swinehart, "The Beer-Lambert Law," *J. Chem. Educ.*, vol. 39, no. 7, Jul. 1962, Art. no. 333, doi:10.1021/ed039p333.
[25] H. W. Siesler, Y. Ozaki, S. Kawata, and H. M. Heise, *Near-Infrared Spectroscopy: Principles, Instruments, Applications*. Hoboken, NJ, USA: Wiley, 2008.
[26] C. Strandman, L. Rosengren, H. G. A. Elderstig, and Y. Backlund, "Fabrication of 45° mirrors together with well-defined v-grooves using wet anisotropic etching of silicon," *J. Microelectromech. Syst.*, vol. 4, no. 4, pp. 213–219, Dec. 1995, doi:10.1109/84.475548.
[27] D. Resnik, D. Vrtacnik, U. Aljancic, M. Mozek, and S. Amon, "The role of Triton surfactant in anisotropic etching of $\{110\}$ reflective planes on (100) silicon," *J. Micromech. Microeng.*, vol. 15, no. 6, Jun. 2005, Art. no. 1174, doi:10.1088/0960-1317/15/6/007.
[28] K. Rola, K. Ptasinski, A. Zakrzewski, and I. Zubel, "Characterization of 45° micromirrors fabricated by silicon anisotropic etching in solutions containing different organic additives," *Procedia Eng.*, vol. 47, pp. 510–513, 2012, doi:10.1016/j.proeng.2012.09.196.
[29] N. P. Ayerden, M. Ghaderi, and R. F. Wolffenbuttel, "Design and fabrication of 45° inclined mirrors for wafer-level optical absorption spectroscopy," *J. Phys., Conf. Ser.*, vol. 757, no. 1, Nov. 2016, Art. no. 012018, doi:10.1088/1742-6596/757/1/012018.
[30] S. K. Rotich, J. G. Smith, A. G. R. Evans, and A. Brunnschweiler, "Photoresist parabolas for curved micromirrors," *J. Micromech. Microeng.*, vol. 8, no. 2, pp. 108–110, Jun. 1998, doi:10.1088/0960-1317/8/2/016.
[31] E. Logean *et al.*, "High numerical aperture silicon collimating lens for mid-infrared quantum cascade lasers manufactured using wafer-level techniques," *Proc. SPIE*, vol. 8550, Dec. 2012, Art. no. 85500Q, doi:10.1117/12.981165.
[32] M. Ghaderi *et al.*, "Design, fabrication and characterization of infrared LVOFs for measuring gas composition," *J. Micromech. Microeng.*, vol. 24, no. 8, Aug. 2014, Art. no. 084001, doi:10.1088/0960-1317/24/8/084001.
[33] G. Gagliardi and H.-P. Loock, *Cavity-Enhanced Spectroscopy and Sensing*. New York, NY, USA: Springer, 2014.
[34] D. Romanini *et al.*, "Optical-feedback cavity-enhanced absorption: a compact spectrometer for real-time measurement of atmospheric methane," *Appl. Phys. B, Lasers Opt.*, vol. 83, no. 4, pp. 659–667, Jun. 2006, doi:10.1007/s00340-006-2177-2.
[35] S. W. Sharpe, T. J. Johnson, R. L. Sams, P. M. Chu, G. C. Rhoderick, and P. A. Johnson, "Gas-phase databases for quantitative infrared spectroscopy," *Appl. Spectrosc.*, vol. 58, no. 12, pp. 1452–1461, Dec. 2004, doi:10.1366/0003702042641281.
[36] N. P. Ayerden, G. de Graaf, and R. F. Wolffenbuttel, "Compact gas cell integrated with a linear variable optical filter," *Opt. Express*, vol. 24, no. 3, pp. 2981–3002, Feb. 2016, doi:10.1364/OE.24.002981.
[37] R. R. McLeod and T. Honda, "Improving the spectral resolution of wedged etalons and linear variable filters with incidence angle," *Opt. Lett.*, vol. 30, no. 19, pp. 2647–2649, Oct. 2005, doi:10.1364/OL.30.002647.
[38] L. S. Rothman *et al.*, "The HITRAN 2008 molecular spectroscopic database," *J. Quant. Spectrosc. Radiat. Transfer*, vol. 110, nos. 9/10, pp. 533–572, Jun./Jul. 2009, doi:10.1016/j.jqsrt.2009.02.013.
[39] N. P. Ayerden, M. Ghaderi, P. Enoksson, G. de Graaf, and R. F. Wolffenbuttel, "A miniaturized optical gas-composition sensor with integrated sample chamber," *Sens. Actuators B, Chem.*, vol. 236, pp. 917–925, Nov. 2016, doi:10.1016/j.snb.2016.03.081.
[40] A. Emadi, H. Wu, S. Grabarnik, G. de Graaf, and R. F. Wolffenbuttel, "Vertically tapered layers for optical applications fabricated using resist reflow," *J. Micromech. Microeng.*, vol. 19, no. 7, Jul. 2009, Art. no. 074014, doi:10.1088/0960-1317/19/7/074014.
[41] N. P. Ayerden, M. Ghaderi, G. de Graaf, and R. F. Wolffenbuttel, "Optical design and characterization of a gas filled MEMS Fabry-Perot filter," *Proc. SPIE*, vol. 9517, Jul. 2015, Art. no. 95171N, doi:10.1117/12.2178773.
[42] G. W. F. Drake, *Springer Handbook of Atomic, Molecular, and Optical Physics*. New York, NY, USA: Springer, 2006.
[43] D. D. Arslanov *et al.*, "Optical parametric oscillator-based photoacoustic detection of hydrogen cyanide for biomedical applications," *J. Biomed. Opt.*, vol. 18, no. 10, Oct. 2013, Art. no. 107002, doi:10.1117/1.JBO.18.10.107002.

N. Pelin Ayerden (S'13–M'16) received the M.Sc. degree from Koc University, Istanbul, Turkey, in 2012, and the Ph.D. degree from the Delft University of Technology, Delft, The Netherlands, in 2016, both in electrical engineering. During her M.Sc. studies, she was involved in the development of a MEMS interferometer-based benchtop FTIR spectrometer. For her Ph.D. studies, she developed a wafer-level microspectrometer in the mid-infrared.

She is currently a Postdoctoral Researcher with the Delft University of Technology. Her research interests include optical MEMS, spectroscopy, and photonics.

Dr. Ayerden received the Best Student Paper Award at SPIE Photonics Europe in 2016.

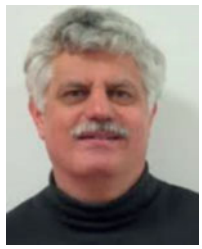

Reinoud F. Wolffenbuttel (SM'93) received the M.Sc. and Ph.D. degrees in electrical engineering from the Delft University of Technology, Delft, The Netherlands, in 1984 and 1988, respectively.

He is with the Delft University of Technology, and is involved in instrumentation and measurement in general and on-chip functional integration of CMOS circuits and silicon sensors, microfabrication in silicon, and the design of optical microsystems in particular. He has published more than 500 papers in international conference proceedings and peer-reviewed journals on these subjects. He was a Visitor at the University of Michigan, Ann Arbor, MI, USA in 1992, 1999, and 2001, at Tohoku University, Sendai, Japan, in 1995, and at EPFL Lausanne, Lausanne, Switzerland, in 1997.

Dr. Wolffenbuttel received the 1997 NWO Pioneer Award. He served as General Chairman of the Dutch National Sensor Conference in 1996, Eurosensors in 1999, and MicroMechanics Europe in 2003.